> AWPL-11-23-2768 <

A Broadband Dual-Polarized ME-Dipole Antenna Array for Millimeter-Wave Applications

Xinzhe Lu, Fan Wu, *Member, IEEE*, Zhi Hao Jiang, *Member, IEEE*, Zhengbo Jiang, *Member, IEEE*, Kin-Fai Tong, *Fellow, IEEE* and Wei Hong, *Fellow, IEEE*

***Abstract*—A magneto-electric dipole implemented using substrate integrated blocks (SIBs) is proposed for broadband dual-polarized array application. Facilitated by the SIB-based design approach, an interlaced arrangement of the perpendicular feeding probes is developed for dual-polarization excitation. While maintaining the wideband feature and single-layered antenna structure, nearly identical radiation characteristics for the two polarizations have been achieved. Additionally, the enlarged probe-to-probe distance increases the degree of design freedom for the feeding network. As a proof-of-concept, a 3 × 3 single-layered antenna array fed by single-layered dual-polarization microstrip-line feeding network is designed and fabricated at the 5G millimeter-wave frequency band. The measured results indicate that the array prototype has a wide overlapped impedance bandwidth of 36.2% covering from 21.3 to 30.7 GHz, within which a maximum gain of 14.7 dBi and a gain variation of 2 dB are maintained. The broadband performance, single-layered radiating structure, and nearly identical performance of two polarizations make the proposed design attractive for applications including 5G and beyond.**

***Index Terms*—Broadband, dual-polarization, millimeter-waves, magneto-electric dipole antenna, microstrip-line feeding network.**

I. Introduction

The increasing demand for wireless communication systems characterizing low-latency and high system capacity has propelled the elevation of communication frequency, especially the exploration of 5G millimeter-wave (mmW) bands. Several 5G frequency range 2 (FR2) operating bands have already been standardized [1]. Therefore, research on broadband mmW antenna arrays holds significant importance in achieving high system capacity and addressing the increased path loss associated with 5G mmW high-frequency transmission. Particularly, considering the integration requirements with 5G devices, a pressing demand arises for wideband mmW antenna arrays with advantages of simple structure, low cost, and stable radiation performance [2]. Simultaneously, dual-polarization characteristic is required to mitigate the multipath fading effects at high frequencies and minimize polarization mismatch.

Over the past decade, sustained research has been conducted on the development of mmW dual-polarized antenna arrays. Slot and patch antennas have undergone substantial developments at mmW dual-polarized antennas [3-6]. These designs, while simple in structure, can only achieve narrow impedance bandwidths of around 10%. Afterward, by adopting feeding techniques based on substrate-integrated waveguide (SIW) structure, cross-slot coupling, or orthogonal aperture-coupled stripline, the operating bandwidth of mmW dual-polarized antenna arrays have been extended to about 20% [7-9]. However, the structures of these antenna arrays are relatively complex, featuring a comparatively high profile or an excessive number of substrate layers, which are not feasible for deployment in portable 5G devices.

Magneto-electric (ME) dipole antennas, with a wide impedance bandwidth and stable radiation performance, are competitive solution to achieve mmW antenna arrays [10-19]. By using SIW feeding structures, mmW dual-polarized ME-dipole antenna arrays have been realized in [11, 12]. Unfortunately, in these SIW-fed antennas, the bandwidth limitation of SIW feeding structure curtails the further expansion of the achievable bandwidth of the antenna. Subsequently, by utilizing crossed L-shaped probes, wideband dual-polarized ME-dipole antenna arrays, which achieve impedance bandwidths of over 40%, are reported in [13, 14]. However, the implementation of such dual-polarization feeds and power-dividing network requires rather complex multi-layer structure that increases the fabrication cost.

In this paper, based on the ME dipole implemented using metallic blocks in [20], a block-shaped structure named substrate integrated block (SIB) is proposed. The SIB is a substrate-integrated form of the metallic blocks. By introducing the SIB, a broadband dual-polarized ME-dipole antenna array is presented. The dual-polarized radiation is excited by using two groups of interlaced perpendicular L-shaped feeding probes. As such, balanced radiation performances for the two polarizations can be achieved, and both the antenna structure and feeding networks can be implemented on a single layer. Compared to previously reported work, this design requires only two substrate layers, providing notable advantages of simple structure and low cost. The measured results of the proposed array show a wide overlapped impedance bandwidth of 36.2%, as well as a stable

Manuscript received XXXX. This work was supported in part by National Natural Science Foundation of China under Grants 62122019, 62293492, 61901106, and in part by the National Key Research and Development Plan under Grant 2023YFB2906103. *(Corresponding authors: Fan Wu; Zhengbo Jiang.)*

X. Lu, F. Wu, Z. H. Jiang, Z. Jiang, and W. Hong are with the State Key Laboratory of Millimeter Waves, School of Information Science and Engineering, Southeast University, Nanjing, 210096, China (e-mail: weihong@seu.edu.cn).

K. -F. Tong is with the department of Electronic and Electrical Engineering, University College London, London, United Kingdom (e-mail: k.tong@ucl.ac.uk).

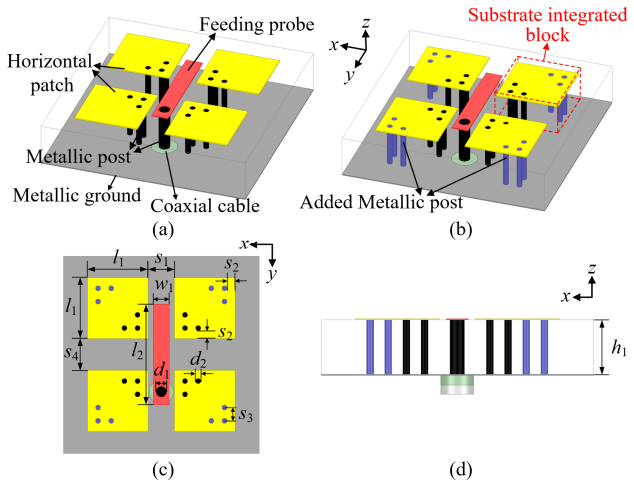

Fig. 1. (a) Perspective view of a conventional LP ME dipole. Geometry of the proposed ME dipole: (b) perspective view, (c) top view and (d) side view. Dimensions are l_1 = 2.3, l_2 = 3.5, s_1 = 0.95, s_2 = 0.15, s_3 = 0.5, s_4 = 1.2, w_1 = 0.6, d_1 = 0.4, d_2 = 0.2, h_1 = 1.575 (unit: mm).

gain in the operational frequency range, which covers the 5G FR2 bands n257, n258 and n261.

II. ME-Dipole Antenna Element

The proposed ME dipole is designed on a piece of TLY-5 substrate with ε_r = 2.2 and is fed by a coaxial cable, as shown in Figs. 1(b), (c) and (d). The operational mechanism of the proposed design can be explained by starting with a conventional linearly-polarized (LP) ME dipole that consists of four square patches, four sets of metallic posts connecting the patches with the metallic ground and an L-shaped probe, as shown in Fig. 1(a). The patches situated on the upper surface of the substrate are employed to form a pair of electric dipoles. The metallic posts, functioning as vertical metallic walls, creating a magnetic dipole in conjunction with the metallic ground plane. The L-shaped probe is centrally positioned for the purpose of excitation.

A minor yet crucial modification is then introduced to this conventional design for broadband dual-polarization array application. As shown Fig. 1(b), by adding additional sets of metallic grounding posts at the opposite diagonal corners of the square patches, four SIBs can therefore be realized. The proposed SIBs still offer similar current paths that allow the realizations of both the E- and M-dipoles, as demonstrated by the simulated current distributions and electric fields of the antenna over a quarter periodic of time (T/4) shown in Fig. 2. When t = 0, the current on the horizontal patches reaches its maximum, and the electric fields at the aperture of the gap are weak. When t = T/4, the currents are primarily distributed on the metallic posts near the center that serve as the metallic wall, and the electric fields at the aperture are strong. These simulated fields distributions indicate that the proposed ME dipole works properly as expected since the E- and M-dipole are both rightly excited. However, it should be noted that the newly added metallic posts at the four outside corners of the ME dipole would result in grounding of the patches at the tails, introducing perturbations to not only the E-dipole but also the

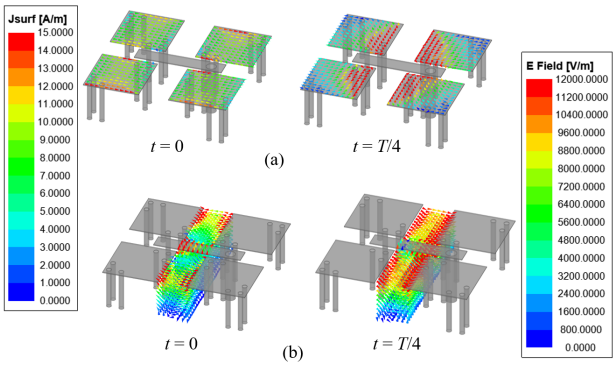

Fig. 2. Simulated current distributions and electric fields of the proposed ME-dipole antenna at 26 GHz: (a) current distributions and (b) electric fields at different times.

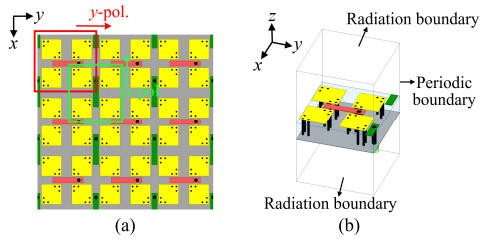

Fig. 3. Configuration of the dual-polarization design: (a) the two-dimensional array (top view) and (b) the unit cell.

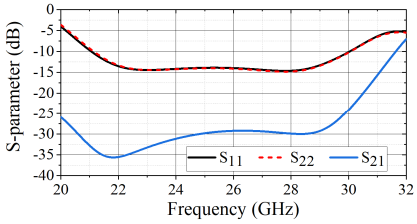

Fig. 4. Simulated S-parameters of the proposed element in infinite array environment.

M-dipole. This would primarily lead to a shift of the operational frequency of the ME dipole. But nearly the same impedance bandwidth compared to the original design can be secured if the geometry is well optimized for a good matching.

To demonstrate the feasibility of constructing a dual-polarized array using the proposed design, the element is employed to design a two-dimensional array, as shown in Fig. 3(a). By adopting two groups of perpendicularly oriented and interlaced probes, orthogonal linear polarizations can be obtained. In contrast to the conventional dual-polarization feeding approach [13, 14], where the perpendicular probes are placed in close proximity, the probes here are designed to be physically distanced from each other by roughly half of the element spacing, facilitating the implementation of dual-polarization feeding structures and networks in a simpler manner (shown later in Section III). Besides, the introduction of the SIBs makes the radiating structure seen by the two groups of perpendicular probes identical, as indicated by the red and green boxes shown in Fig. 3(a), which leads to similar performances including the gain and bandwidth for the two polarizations. The corresponding unit cell for fast evaluation of element performance in array can be found in Fig. 3(b). The

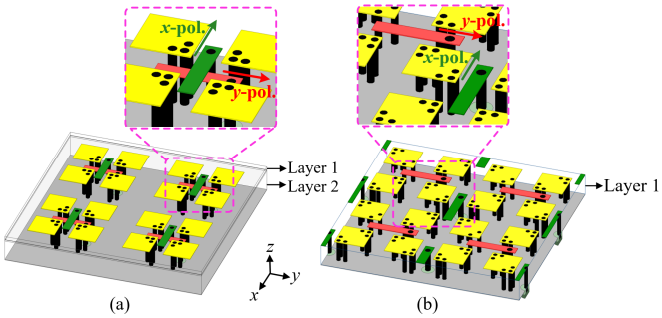

Fig. 5. Comparison of two feeding structures for dual-polarized array: (a) the conventional design and (b) the design proposed in this work.

simulated S-parameters at the two feeding ports in one unit cell are shown in Fig. 4. The simulated results indicate that the proposed ME dipole achieves an overlapped -10 dB impedance bandwidth of 35.1%, spanning from 21.05 to 30 GHz. The mutual coupling between the two ports is found to be lower than -25 dB in the frequency range of interest.

III. Dual-Polarized ME-Dipole Antenna Array

A. Design and Implementation of the Dual-polarized Array

A conceptual drawing of the proposed dual-polarized array is plotted in Fig. 5(b) and is compared with one typical conventional design [14] shown in Fig. 5(a). In the conventional approach, the crossed feeding probes are situated at the center of one antenna element, leading to a small probe-to-probe distance and the need of additional copper layer for avoiding direct contact of the two perpendicular probes. In contrast, in the proposed design, the distance between the adjacent perpendicular probes is greatly enlarged. As such, the feeding probes for both polarizations can be designed on the same copper layer, thereby reducing the total substrate layers with simplified structure. Another notable advantage of this arrangement is that the enlarged distance between orthogonal feeding probes makes the implementation of dual-polarization feeding networks in a single layer more practical.

As a proof-of-concept validation, a 3 × 3 dual-polarized ME-dipole array is designed, as illustrated in Fig. 6(a). The horizontal portion of the probes and patches are printed on the top side, while the microstrip-line feeding networks are distributed on the bottom surface. An adhesive thin film (Rogers RO4450F) was used to bond the two layers together. By employing nine probes for each polarization to excite the elements, this layout generates a 3 × 3 ME-dipole array for each of the two polarizations. The dimensions of the antenna elements are fine-tuned in the array design to keep a good matching. The optimized element spacing is 6.55 mm (0.57 λ_0) in both of the two directions, where λ_0 is the free space wavelength at center frequency f_0 (26 GHz).

As shown in Fig. 6(b), the microstrip-line feeding network, i.e., the one-to-nine power divider, is designed by cascading several one-to-three equal power dividers. Thanks to the interlaced probe arrangement, two identical feeding networks for launching the two orthogonal polarizations can be realized on the same layer.

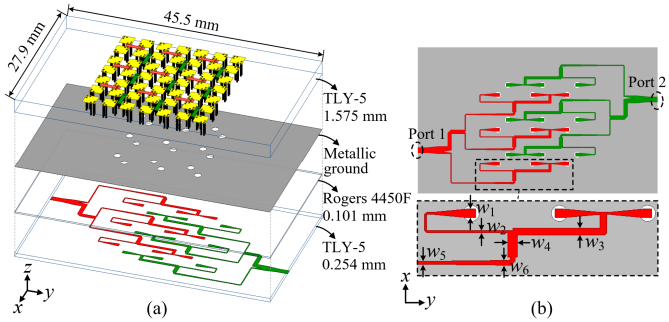

Fig. 6. Configuration of the dual-polarized antenna array: (a) exploded view of the whole array and (b) the microstrip-line feeding networks (bottom view). Dimensions of the feeding networks are w_1 = 0.64, w_2 = 0.17, w_3 = 0.5, w_4 = 0.7, w_5 = 0.17, w_6 = 0.36 (unit: mm).

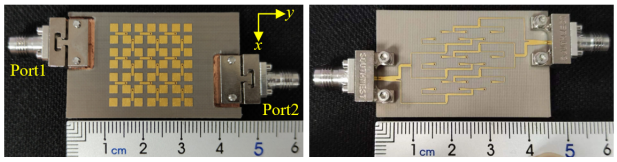

Fig. 7. Photographs of the prototype: (a) top view and (b) bottom view.

B. Experimental Characterization

A prototype of the 3 × 3 ME-dipole array, measuring a 46 × 28 mm^2 physical size (4 × 2.4 λ_0^2), was fabricated to experimentally validate the methodology. As shown in Fig. 7, a section of the top substrate of the prototype is removed to expose the underlying metallic ground plane by computer numerical control machining, for the purpose of realizing better contact of the connectors with the antenna ground plane.

A network analyzer was employed to measure the reflection coefficients, while the array performances were characterized in a far-field chamber. S-parameters and gains of the array are depicted in Fig. 8. Good agreement between the simulated and measured S-parameters can be observed. The measured results showcase an overlapped -10 dB bandwidth of 36.2% (from 21.3 to 30.7 GHz), with the |S21| less than -22.5 dB in the same frequency range.

The measured gain is up to 14.7 and 14.6 for *x*- and *y*-polarizations, respectively. The simulated and measured results show similar trends as frequency changes, though the measured results are slightly lower than the simulated ones from 26 to 31 GHz. The inconsistency is suspected to be caused by the fabrication uncertainties. Besides, the variation of gain is within 2 dB in the operational frequency range.

Figs. 9 and 10 illustrate the simulated and measured radiation patterns of the two polarizations at 21.5 GHz, 26 GHz and 30.5 GHz. The results agree well with each other in terms of the beamwidth and the sidelobe level. The beamwidth of the main lobe gradually decreases as the frequency increases. The side lobe level remains below -10 dB for both of the two polarizations across the operating band. The cross-polarization at main beam directions is lower than -13 dB at 21.5 and 26 GHz and around -11 dB at 30.5 GHz. In addition, the two polarizations show similar performance, but with slight differences in side lobe level and cross-polarization. As

TABLE I
COMPARISON OF THE ARRAY IN THIS WORK AND THOSE IN REFERENCES.

Ref.	Array element	Array size	Number of radiating structure layers	Number of feeding network layers	Impedance bandwidth (%)	Isolation (dB)	Peak gain (dBi)	Gain variation (dB)	Aperture efficiency at f_0 (%)
[7]	Slot	8 × 8	1	2	17.1	35	22.3	2.6	46.3
[8]	Patch	4 × 4	1	2	18.6	33	18	3.5	34.2
[11]	ME dipole	2 × 2	1	2	22	15	12.5	2	42.8
[12]	ME dipole	1 × 8	4	2	21	45	16.1	2.3	64.5
[14]	ME dipole	1 × 4	3	1	47.1	18	12.06	4	71.6
This work	ME dipole	3 × 3	1	1	36.2	22.5	14.7	2	67.5

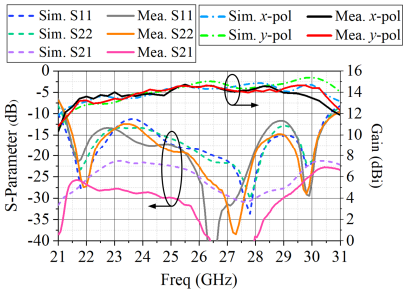

Fig. 8. S-parameters and gains of the 3 × 3 ME-dipole antenna array.

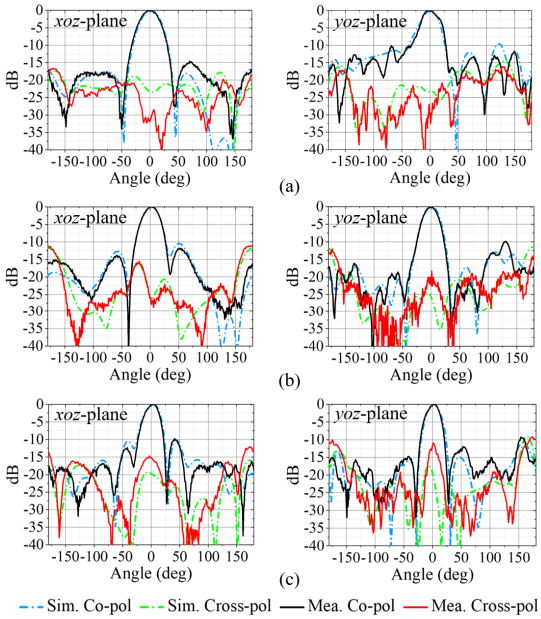

Fig. 9. Normalized radiation patterns of the antenna array when port 1 (*y*-polarization) is excited: (a) 21.5 GHz, (b) 26 GHz and (c) 30.5 GHz.

shown in Fig. 6, the two feeding networks can be regarded as placed along the *y*-axis, while the two sets of probes are placed along the *x*- and *y*-axis, respectively. The discrepancy between the radiation patterns of the two polarizations can be attributed to the difference in the relative positions of their radiating structures and feeding networks.

C. Discussion

The configurations and performance metrics of previously published dual-polarized antenna array designs are summarized and compared with the proposed work in Table I.

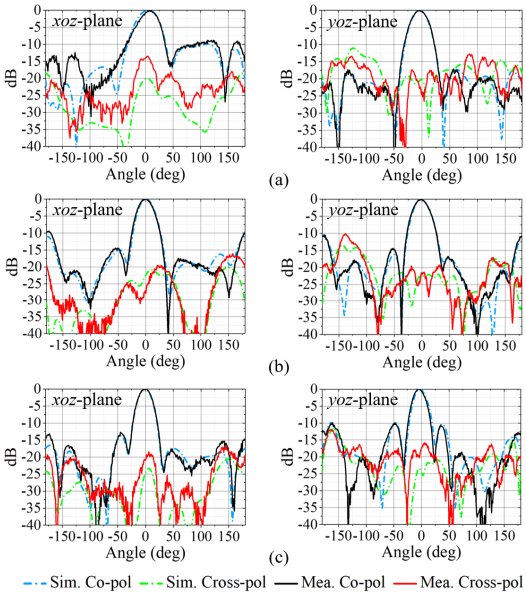

Fig. 10. Normalized radiation patterns of the antenna array when port 2 (*x*-polarization) is excited: (a) 21.5 GHz, (b) 26 GHz and (c) 30.5 GHz.

Compared with designs reported in [7], [8], [11] and [12], this work shows a wider impedance bandwidth of 36.2%. Benefitting from the SIB-based design approach and interlaced perpendicular feeding probes, the proposed array has less substrate layers than the reported designs, which is cost-effective and easier to fabricate. Moreover, the nearly identical array performances for the two polarizations are also obtained, further balancing the performance of gain stability and bandwidth.

IV. CONCLUSION

A broadband dual-polarized 3 × 3 ME-dipole antenna array has been proposed in this work for mmW application. By utilizing the SIBs and interlaced perpendicular feeding probes, the array achieves balanced dual-polarization performances within a wide frequency range in a simple structure. The fabricated prototype experimentally demonstrates an overlapped impedance bandwidth of 36.2%, a maximum gain of 14.7 dBi and a gain variation less than 2 dB. The attractive dual-polarization characteristics as well as the single-layered radiating structure make the proposed array competitive for many portable applications.

REFERENCES

[1] *Technical Specification Group Radio Access Network; NR; User Equipment (UE) Radio Transmission and Reception; Part 5: Satellite Access Radio Frequency (RF) and Performance Requirements (Release 18),* 3GPP TS 38.101-5, V18.3.0, Sept. 2023.

[2] X. Shen, Y. Liu, L. Zhao, G. -L. Huang, X. Shi and Q. Huang, "A miniaturized microstrip antenna array at 5G millimeter-wave band," *IEEE Antennas Wireless Propag. Lett.*, vol. 18, no. 8, pp. 1671-1675, Aug. 2019.

[3] J.-C. S. Chieh, B. Pham, A.-V. Pham, G. Kannell, and A. Pidwerbetsky, "Millimeter-wave dual-polarized high-isolation antennas and arrays on organic substrates," *IEEE Trans. Antennas Propag*., vol. 61, no. 12, pp. 5948–5957, Dec. 2013.

[4] T. Chaloun, V. Ziegler, and W. Menzel, "Design of a dual-polarized stacked patch antenna for wide-angle scanning reflectarrays," *IEEE Trans. Antennas Propag.*, vol. 64, no. 8, pp. 3380–3390, Aug. 2016.

[5] J. Lu et al., "Broadband dual-polarized waveguide slot filtenna array with low cross polarization and high efficiency," *IEEE Trans. Antennas Propag*., vol. 67, no. 1, pp. 151–159, Jan. 2019.

[6] Q. Yang et al., "Differentially-fed dual-polarized 2D multibeam antenna array for millimeter-wave applications," in *Proc. Int. Conf. Microw. Millimeter Wave Technol.* (*ICMMT)*, 2020, pp. 1-3.

[7] Z. Chen, H. Liu, J. Yu, and X. Chen, "High gain, broadband and dual-polarized substrate integrated waveguide cavity-backed slot antenna array for 60 GHz band," *IEEE Access*, vol. 6, pp. 31012–31022, 2018.

[8] Md. A. Islam and N. C. Karmakar, "A 4 × 4 dual polarized mm-wave ACMPA array for a universal mm-wave chipless RFID tag reader," *IEEE Trans. Antennas Propag*., vol. 63, no. 4, pp. 1633–1640, Apr. 2015.

[9] X. Tong, Z. H. Jiang, C. Yu, F. Wu, X. Xu, and W. Hong, "Low-profile, broadband, dual-linearly polarized, and wide-angle millimeter-wave antenna arrays for Ka-band 5G applications," *IEEE Antennas Wireless Propag. Lett*., vol. 20, no. 10, pp. 2038–2042, Oct. 2021.

[10] H. Wong and K. -M. Luk, "Unidirectional antenna composed of a planar dipole and a shorted patch," in *Proc. Asia-Pacific Microw. Conf.*, 2006, pp. 85-88.

[11] Y. Li and K.-M. Luk, "60-GHz dual-polarized two-dimensional switch-beam wideband antenna array of aperture-coupled magneto-electric dipoles," *IEEE Trans. Antennas Propag*., vol. 64, no. 2, pp. 554–563, Feb. 2016.

[12] A. Li, K.-M. Luk, and Y. Li, "A dual linearly polarized end-fire antenna array for the 5G applications," *IEEE Access*, vol. 6, pp. 78276–78285, 2018.

[13] Y. Li, C. Wang, and Y. X. Guo, "A Ka-band wideband dual-polarized magnetoelectric dipole antenna array on LTCC," *IEEE Trans. Antennas Propag*., vol. 68, no. 6, pp. 4985–4990, Jun. 2020.

[14] Y. C. Chang, C. C. Hsu, M. I. Magray, H. Y. Chang, and J.-H. Tarng, "A novel dual-polarized wideband and miniaturized low profile magneto-electric dipole antenna array for mmWave 5G applications," *IEEE Open J. Antennas Propag*., vol. 2, pp. 326–334, 2021.

[15] J. Wang et al., "A low-profile vertically polarized magneto-electric monopole antenna with a 60% bandwidth for millimeter-wave applications," *IEEE Trans. Antennas Propag*., vol. 69, no. 1, pp. 3–13, Jan. 2021.

[16] J. Wang et al., "Millimeter-wave wideband endfire magnetoelectric dipole antenna fed by substrate integrated coaxial line," *IEEE Trans. Antennas Propag*., vol. 70, no. 3, pp. 2301–2306, Mar. 2022.

[17] J. Wang et al., "A leaky-wave magnetoelectric antenna with endfire radiation for millimeter-wave communications," *IEEE Trans. Antennas Propag*., vol. 71, no. 4, pp. 3654–3659, Apr. 2023.

[18] L. Cai, H. Wong and K. -F. Tong, "A simple low-profile coaxially-fed magneto-electric dipole antenna without slot-cavity," *IEEE Open J. Antennas Propag.*, vol. 1, pp. 233-238, 2020.

[19] L. Cai and K. -F. Tong, "A single-fed wideband circularly polarized cross-fed cavity-less magneto-electric dipole antenna," *Sensors*, vol. 23, no. 3, p. 1067, Jan. 2023.

[20] K. M. Luk et al., "A microfabricated low-profile wideband antenna array for terahertz communications," *Sci Rep*, vol. 7, no. 1, p. 1268, Apr. 2017.